Structures 61 (2024) 105981

Contents lists available at ScienceDirect

Structures

journal homepage: www.elsevier.com/locate/structures

The effect of continuity reinforcement on the progression of collapse in reinforced concrete buildings

Nirvan Makoond [a,*], Andri Setiawan [a], Sarah L. Orton [b], Jose M. Adam [a]

[a] ICITECH, Universitat Politècnica de València, Camino de Vera s/n, 46022 Valencia, Spain
[b] University of Missouri-Columbia, E2503 Lafferre Hall, Columbia, MO 65211, USA

ARTICLE INFO

Keywords:
Progressive collapse
Disproportionate collapse
Robustness
Buildings
Alternative Load Paths
Continuity
Segmentation

ABSTRACT

Research performed on the progressive collapse of reinforced concrete buildings has led to the development of several design approaches relying on sufficient continuity reinforcement to provide alternative load paths that can prevent collapse after the failure of single columns. However, there are very few works examining the possible contribution that continuity reinforcement could have in pulling down parts of a structure that would otherwise be unaffected after large initial failures. This article presents the findings of a study based on validated simulations of a prototype building using the Applied Element Method (AEM). The results reveal that a large amount of continuity reinforcement can indeed contribute to more failure propagation after very large initial failures by transmitting more unbalanced forces to columns. It is also demonstrated that localised reductions in continuity reinforcement can prevent failure propagation after large initial failures. In addition, it is shown that this can be achieved while still allowing alternative load paths to develop after single-column failure as required by current codes and guidelines.

1. Introduction

The collapse of the Ronan Point tower in London in 1968 led to a significant increase in awareness within the structural engineering community on the importance of incorporating redundancy within a structural system in order to prevent progressive collapse. The findings of the investigation that ensued first led to the incorporation of prescriptive tying force requirements in the British Code of Practice 110 in 1972 [1]. Since then, a number of recommendations and requirements aiming to improve the robustness of reinforced concrete (RC) buildings have been included in guidelines [2–5] and standards [6–10] issued in different parts of the world. As a result, different design approaches are now available to engineers for improving the structural robustness of RC building structures.

The two most commonly employed methods to achieve structural robustness are prescriptive tying force requirements and the alternative load path method (ALPM) [7,9]. The former is an indirect design approach which involves ensuring that continuous horizontal and vertical reinforcing elements are present within a building design and that these elements are able to withstand a certain notional load which is related to the gravity loads for which they are designed. On the other hand, the ALPM is a direct design approach in which engineers have to explicitly verify that a structural system is able to withstand the removal of different individual vertical loadbearing elements. Although the application of these two design approaches can lead to different building designs [11], they fundamentally aim to ensure that loads supported by a failed element can be redistributed to other parts of a structure through continuous reinforcement.

Naturally, this approach to designing against progressive collapse stems from previous research that has been performed in this field, the vast majority of which has focused on studying the removal of single columns, either through experiments [12–14] or computational simulations [15]. While providing more continuity to ensure load redistribution is undoubtedly a good strategy to avoid collapse after the failure of a single column [16,17], it could also contribute to increasing the risk of disproportionate collapse should a larger initial failure occur. In such situations, having extensive continuity can contribute to a collapsing part pulling down parts of a building that would otherwise be unaffected. In fact, this phenomenon is well known by demolition experts and even employed when performing implosions [18].

While there is only a small probability of occurrence of a large initial failure that may lead to the pulling down of the remaining structure,

* Corresponding author.
E-mail address: ncmakoon@upv.es (N. Makoond).

https://doi.org/10.1016/j.istruc.2024.105981
Received 23 September 2023; Received in revised form 22 January 2024; Accepted 26 January 2024
Available online 8 February 2024

there do exist several actual cases demonstrating such initial failures [19]. The possibility of a large initial failure is increased due to the fact that building collapses almost always involve a multitude of interacting causal factors including deterioration and change of use, as well as design and construction errors. In fact, a recent review showed that occurrences of progressive collapse triggered by the failure of more than two columns occurred in over 57% of cases [19].

Since current guidelines such as the ALPM do not address large initial failures, different design strategies need to be developed in order to ensure improved structural performance should a large initial failure arise during a building's lifetime. In this regard, methods based on isolating collapse to a specified spatial extent by segmenting it in different parts could prove to be particularly effective. Among the conceivable ways for achieving segmentation [20] exists the possibility of using expansion joints. However, this could be counterproductive as it involves completely interrupting continuity, which has been shown to work well for small initial failures. A more promising approach for segmenting buildings involves using structural fuses to connect different building segments. Such fuses should be able to ensure load redistribution under normal operational conditions (and for small initial failures), but separate when larger failure propagation is inevitable. Although the likely benefits of such an approach have been envisaged by researchers [20–23] and even in guidelines issued by the National Institute of Standards and Technology [4], a fundamental understanding of how it could contribute to arresting failure propagation in RC buildings has not yet been established.

While designing for segmentation is the overall goal, first and foremost, it is crucial to better understand when and how increasing continuity reinforcement may contribute to a more disproportionate collapse or the pulling down of the remaining structure. To achieve this, it is necessary to study structural responses beyond the secondary resisting mechanisms that can prevent the initiation of collapse. There do exist studies in literature that have analysed the consequences of different possible failure modes [24], or the effect of multiple-column loss [25] and more distributed partial initial damage [26]. However, all these studies have relied on simplified structural analysis or modelling strategies that cannot capture relevant phenomena that occur after a collapse has initiated. In addition, to the best of the author's knowledge, no works have ever studied the situations in which continuity reinforcement may contribute to increasing disproportionate collapse risk.

To address this gap, this article presents an analysis of how continuity reinforcement can contribute to collapse propagation using validated computational simulations of a realistic building design using the Applied Element Method (AEM). First, the simulation strategy and computational methods employed for the study are briefly described and validated against experimental results from literature (Section 2). The design of the prototype building used for the study is then presented in Section 3. Finally, an analysis of the role of continuity in the progression of collapse is provided in Section 4 before summarising the main conclusions that could be drawn from this research.

2. Simulation strategy and validation

The Applied Element Method (AEM) was chosen for performing the analyses presented in this article due to its computational efficiency and ability to accurately represent all phases of a collapse including element separation, contact, and collision [27]. This method relies on discretising a structure in small rigid elements that are connected by distributed normal and shear springs on each face. Each element has six degrees of freedom (three translational and three rotational) at its centre and all constitutive relations as well as contact and collision behaviour are implemented through the distributed springs. As a result, it is significantly less computationally expensive compared to deformable finite elements and particularly suitable for simulating full structures in extreme situations. Despite its simplifying assumptions [28], a large number of comparisons with experimental and theoretical results [27] indicate that the method is able to accurately represent large displacements [29], cyclic loading [30], element separation, contact, and collision [31].

For the analyses to be performed as part of this study, concrete has been modelled using solid elements while reinforcing bars are modelled as specialised springs placed at the exact location of the bars. More details on the constitutive models employed can be found in [27].

Prior to employing the AEM to perform simulations of the prototype building subject of this study (see Section 3), it was used to simulate two different sets of experiments to validate the modelling strategy to be employed. Results from this exercise are presented in the following subsections.

2.1. Subassemblies subjected to column removal

Two 2D-frame subassemblies (beam-column system without slab) tested by Pham and Tan [32] were selected for validating the simulations performed using the AEM. Both subassemblies represented the case of an internal column loss with a 1/3 scale: subassembly FR was subjected to a static pushdown test (with concentrated load), and subassembly FDU2-F/55 was subjected to dynamic column removal (with uniformly distributed load). Both specimens consisted of a double-span beam with a dimension of 100 × 180 mm and a span length of 2.4 m. Hence, the total length of the specimens was 4.8 m. The side columns had a square shape with a side length of 180 mm. The reinforcement configuration and material properties can be consulted in Pham and Tan [32]. Fig. 1 illustrates the test setup and boundary conditions for both tests. Both specimens were horizontally restrained through the extended portion of the beams that were connected to a stiff steel A-frame or strong wall. To simulate the axial forces generated by the gravity loads of the upper parts of the prototype building that were not simulated in the lab, the side columns were post-tensioned using four steel roads connected to a vertical hydraulic jack (applying 200 kN of axial force).

For the FR specimen, the downward displacement was gradually applied using a vertical hydraulic jack positioned at the location of the central column (displacement control). On the other hand, for the FDU2-F/55 specimen, a total gravity load of 55 kN was imposed by hanging steel weights in four beam locations (see Fig. 1), approximating the uniformly distributed load condition. Then, the vertical support in the internal column was removed using a quick-release device to represent a sudden column removal.

Based on this information, numerical models were built and simulations of the tests were performed using the AEM. The main assumptions adopted in the modelling are listed below:

1. The lateral restraints provided by the A-frame or strong wall were represented using horizontal springs with a stiffness value of:
   a. FR specimen: 7848 kN/m (max) – 657 kN/m (min)
   b. FDU2-F/55 specimen: 88,290 kN/m (max) – 3041 kN/m (min)
2. The maximum spring stiffness represents the scenario under arching or catenary conditions, whereas the minimum stiffness represents a very short transition stage between the two mechanisms (from compression to tension). This short transition was assumed to occur for a duration of 0.05 s in the dynamic test.
3. Reinforcement bars were modelled as a spring element with a perfect bond assumption with the surrounding concrete.
4. A uniform element size with an average dimension of 25 mm was used.
5. The load was introduced as an imposed displacement for the FR specimen, whereas the weights applied to the FDU2-F/55 specimen were represented using additional lumped masses at the exact locations from which the steel weights were hung (see Fig. 1).
6. The central column's removal time for the dynamic test was taken as 0.022 s, corresponding to the removal time reported by Pham and Tan [32].

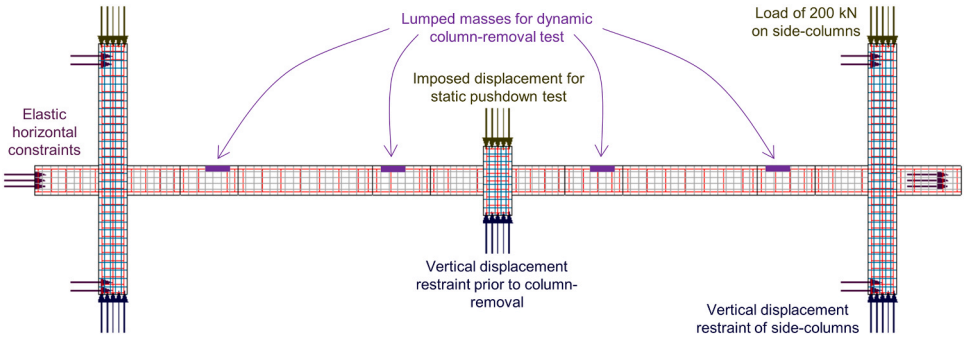

Fig. 1. Basic model configurations employed for AEM simulations of subassembly tests performed by Pham and Tan.

7. Besides damping due to cracking, hysteric behaviour, and friction (considered implicitly in the AEM), an additional external mass proportional damping was calculated based on the frequency of the vertical vibration of the specimen and introduced to the model to generate an equivalent viscous damping of 3.5% to be consistent with the reported value by Pham and Tan [32].

Fig. 2a compares the measured and predicted response of the middle-joint displacement against the vertical load of the FR specimen (quasi-static test). Overall, the AEM predicted the specimen's response reasonably well throughout different phases of the tests: flexure with compressive arching action, the transition from arching to catenary action, and the failure of the catenary action due to rebar fractures. However, bottom rebar fracture occurs earlier (at a smaller vertical displacement) in the AEM simulation. This is possibly caused by the AEM model's perfect-bond assumption, which leads to a higher stress concentration around the cracked regions. In reality, some degree of bond slip is expected to occur around the rebar, which helps to relax and redistribute the stress concentration. This phenomenon eventually delays the fracture. Fig. 2b shows a comparison of the measured and predicted horizontal reaction for the static pushdown test. The general pattern was captured reasonably well by the AEM. However, the decrease of horizontal forces after the peak of arching action and during the transition stage occurred relatively earlier in the model simulation compared to the test. A similar observation was reported by Grunwald et al. [33]. One potential cause is the idealisation of the boundary conditions, particularly the horizontal restraints. The actual test had a complex interaction between the specimen and the horizontal restraining system. Such an interaction is not fully captured using simple horizontal elastic constraints in the AEM simulation.

Fig. 3 compares the measured and predicted responses of the dynamic test of FDU2-F/55. Once again, it can be observed that the decrease of horizontal forces after compressive arching action occurs less gradually in the AEM simulation (Fig. 3c), presumably also due to how the elastic horizontal constraints are represented in the model. Nevertheless, there is still a good agreement between all measured responses, indicating that the AEM simulations can provide a sufficiently accurate representation of the global dynamic structural response. Table 1 summarises the comparison between the measured and predicted responses using the AEM for both tests.

2.2. *Half-scale 3-storey RC frame structure*

The second validation of the AEM aims to test the applicability of the adopted parameters to simulate the behaviour of a full building consisting of multiple beams, columns, and slabs. The test performed by Xiao et al. [34] was selected. The test specimen consisted of a half-scale RC frame building with 3 × 3 bays designed according to ASCE 7–2002 [35] and ACI 318–08 [36] for Seismic Design Category C. The building was designed to withstand a gravity load combination of 1.2DL + 1.6LL, which resulted in 1.44 kN/m^2 of additional superimposed dead load (SIDL) and a live load of 4.77 kN/m^2. More detailed information about the dimensions of the structural components, reinforcement configurations, and material parameters can be consulted in Xiao et al. [34]. The experimental campaign consisted of three tests involving multiple column removals, but only the second test was simulated in this study, involving the removal of two edge (perimeter) columns, D2 and D3 (see Fig. 4). The two columns were removed sequentially during the test, with D3 removed prior to D2. This test was chosen as it was reported to cause the most severe damage to the system, leading to the formation of plastic hinges and eventually to a partial collapse (after 14 min), thus ensuring this validation exercise encompasses relevant phenomena

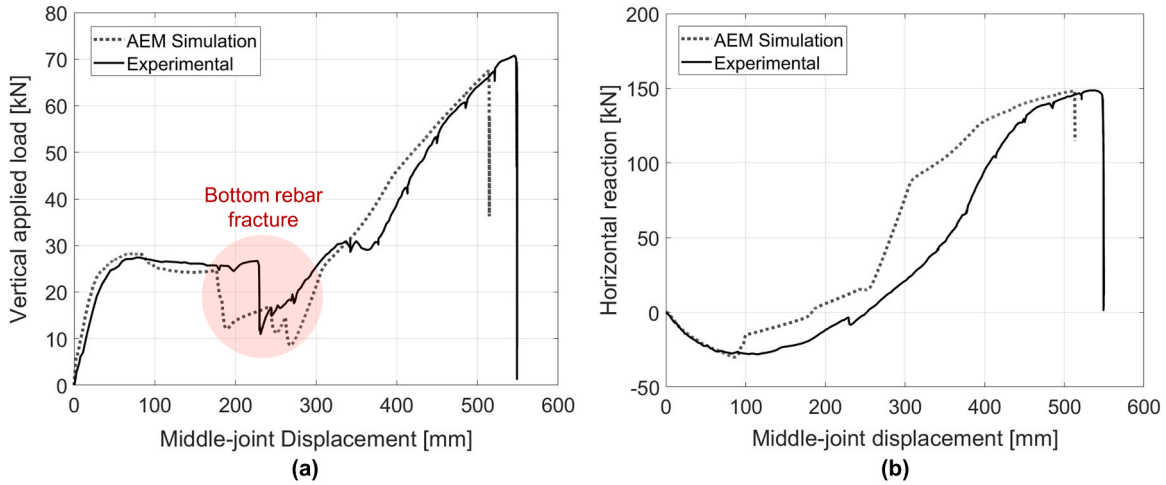

Fig. 2. Comparison of experimental and simulation results for static pushdown test of the FR specimen performed by Pham and Tan [32].

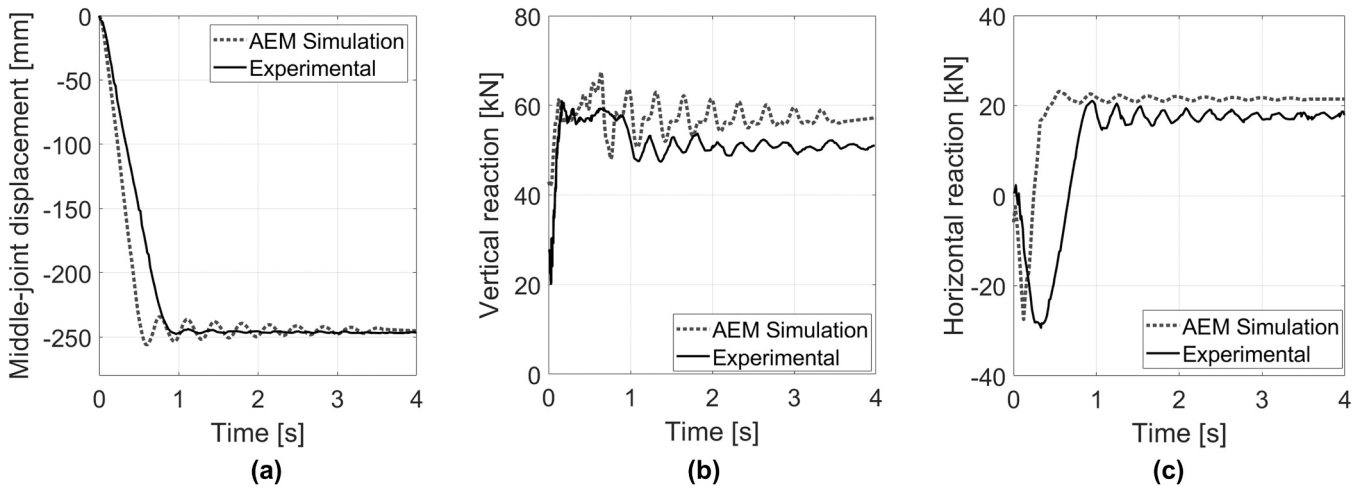

Fig. 3. Comparison of experimental and simulation results for dynamic test of the FDU2-F/55 specimen performed by Pham and Tan [32].

Table 1
Summary of differences between experimental tests and model predictions.

Test	Vibration period [s]			Max. vertical reaction [kN]			Max. horizontal reaction [kN]		
	Test	AEM	Diff.	Test	AEM	Diff.	Test	AEM	Diff.
FR (Static)	-	-	-	70.9	67.7	4%	148.8	148.4	0.3%
FDU2-F/55	0.305	0.292	4%	61.1	57.5	6%	21.2	23.1	-9%

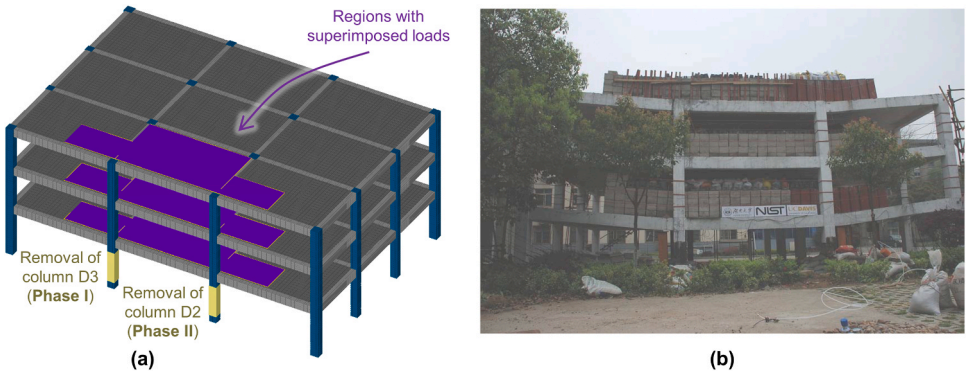

Fig. 4. (a) 3D model used for simulating half-scale structure; (b) View of building after completion of test performed by Xiao et al. (reproduced with permission from [37]).

occurring during the collapse of RC structures. Before removing the columns, a superimposed test load of 20 kN/m^2 was applied to the tributary area associated with the columns to be removed, indicated by the shaded regions in Fig. 4a. The columns were removed using the impact of a steel projectile launched using a hydrogen gas cannon.

The AEM model of the building was constructed using an average element size of 80 mm and adopting the same basic assumptions as employed in the subassembly validation. An important aspect that must be highlighted here is the adoption of fracture energy to control the concrete material's peak and post-peak behaviour under tension and compression. For compression, the fracture energy was determined using the expression proposed by Lertsrisakulrat et al. [38,39]. For tensile behaviour, a fracture energy of 0.180 kN/m was used based on average experimental values from tests reported in [40]. The model with post-peak behaviour controlled by fracture energy (instead of by the critical stress-strain limit) was found to give a better agreement with the measured responses.

Fig. 5 compares the vertical displacements at the removed column locations (D2 and D3) as a function of time. In Fig. 5a, the response measured above the removed column D3 was well captured by the AEM model. However, the predicted response seems to oscillate more than the measured response. This can be due to the previous damage to the structure that occurred during the first test and due to the effect of the concrete blocks used for loading, both of which can result in additional damping that is not well captured in the simulation. Nevertheless, a more remarkable difference can be observed for the second phase of the test, in which D2 was also removed (see Fig. 5b and c). The response of point D2 was captured well, but the vertical displacement of D3 was overestimated by about 10–15 mm in the AEM analysis. One potential explanation is that the AEM simulation performed in this study did not consider the previous removal of columns A1 and B1, located at the corner bay of the building. The AEM assumes that the building was in pristine condition before removing columns D2 and D3, whereas, in reality, the building was partly damaged during the first phase of the tests. Such initial damages and the previous loading in other parts of the structure are believed to cause the asymmetric behaviour of the measured responses of columns D2 and D3. In fact, the actual reason for this asymmetric behaviour is unclear, and has not been addressed by the

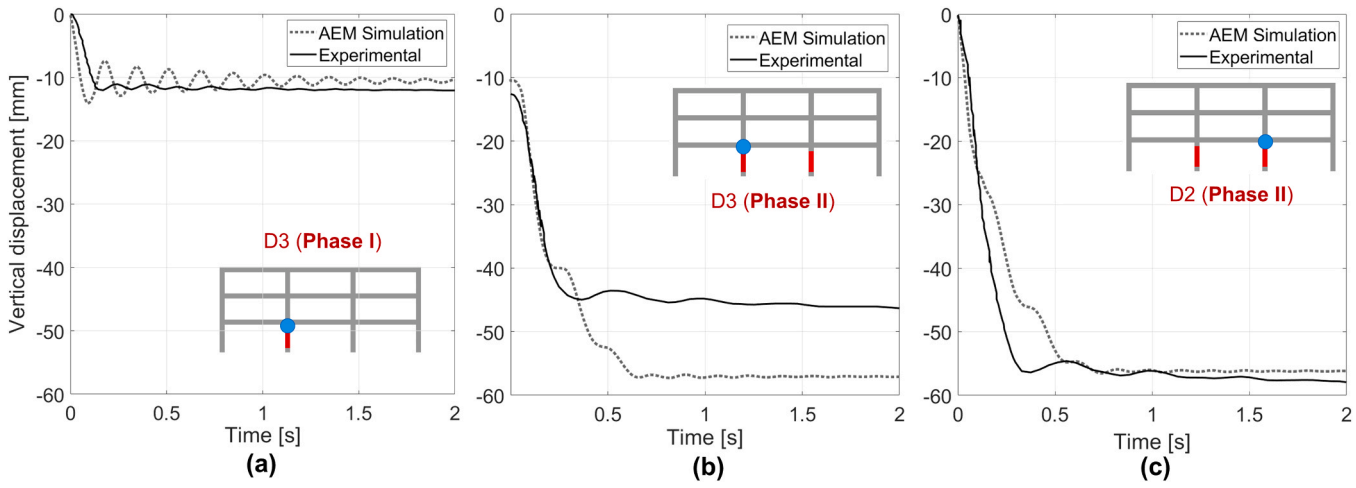

Fig. 5. Comparison of measured and predicted vertical displacements after removal of columns D3 and D2 (Test 2).

authors originally reporting the test, the important point being that this test eventually leads to the partial collapse of this part of the structure after 14 min. The displacement time histories shown in Fig. 5b and c therefore only represent the initial phase of the collapse, with both measured displacements continuing to increase until more than the effective depth of the beams (325 mm) before resting on preset steel shoring columns. Nevertheless, the maximum deflection response (point D2), which should lead to more critical scenarios, was captured accurately by the AEM.

Fig. 6 compares the observed crack patterns with the plots of the principal tensile strains of the AEM. In general, an excellent agreement and consistent yield line pattern can be observed between the two, representing the formation of a failure mechanism. The severity of the crack patterns reported in the test was consistent with the magnitude of the AEM-predicted principal strains. The cracks in the top surface of the slabs represent a tangential crack pattern that overlaps with the beams' and slabs' negative moment regions (activating the top bars) at the surroundings of the removed columns. The two internal columns (C2 and C3) separated by a shorter span length from the removed columns were strained more than the two corner columns (D4 and D1), indicating that most internal force redistribution went through the shortest path. In contrast, a fan-shaped (radial) crack pattern was observed at the bottom surface of the floors. As expected, the highest strain concentration was observed at regions between the two removed columns (D2 and D3), where the sagging (positive) moment was highest. Based on the predicted strains by the AEM simulation, it is evident that the partial collapse of the region surrounded by the cracks shown in Fig. 6 is imminent, as actually occurred in the test. In fact, this is further strengthened by the fact that an AEM simulation with the tensile behaviour of the concrete based on the critical stress-strain limit (instead of fracture energy) leads to a more sudden partial collapse of exactly the same region shown in Fig. 6, suggesting that the early displacement time histories shown in Fig. 5b and c may change depending on highly variable tensile properties of concrete, but that the overall failure mode is well captured by the AEM simulations.

To conclude, the adopted AEM parameters have been proven to produce realistic predictions of the responses of complex 3D buildings. These results justify the applicability of the proposed modelling strategy to conduct a detailed investigation on the role of continuity in collapse propagation (presented in the following sections). It should also be noted that the authors have performed other comparisons with static and dynamic tests involving the (sudden) removal of columns from subassemblies [41] and full-scale structures [42] for the purpose of validating the simulation strategy employed in this research.

3. Prototype building and robustness design

In order to better understand the effect of continuity reinforcement on the potential pulling down of a remaining structure during a collapse, a prototype building was designed with a high level of continuity as prescribed by the method developed for the next generation of Eurocodes [43]. More details on the method and its application to the design of the prototype building are provided in subsection 3.1.

As shown in Fig. 7, the prototype building consisted of 3 × 7 bays with spans of 10 m, and three floors with a height of 4 m each.

The building was designed according to Eurocode 2 [44] with an imposed dead load of 2 kN/m^2 and a live load of 3 kN/m^2. These design loads are appropriate for use categories C3 and lower according to Eurocode 1 [45], which correspond to office areas and certain areas where people are expected to congregate. In addition, a low ductility

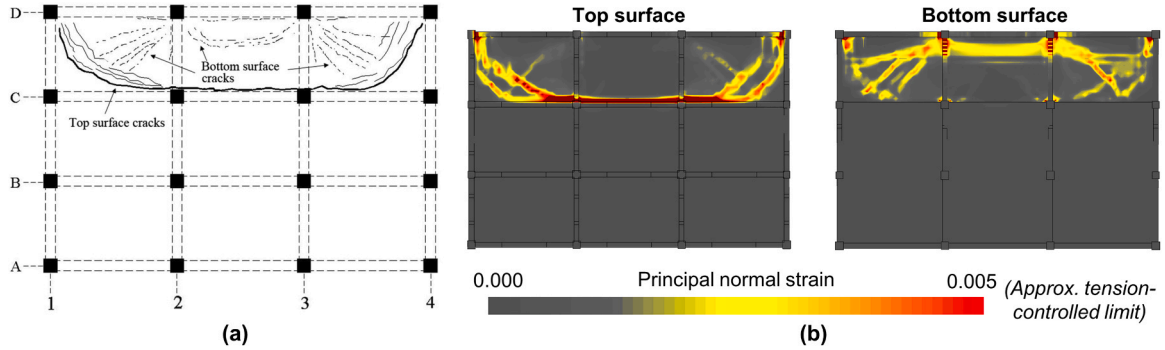

Fig. 6. (a) Observed cracks in partial collapse after removal of columns D3 and D2 [34]; (b) Principal normal strains predicted by AEM simulations of the same test.

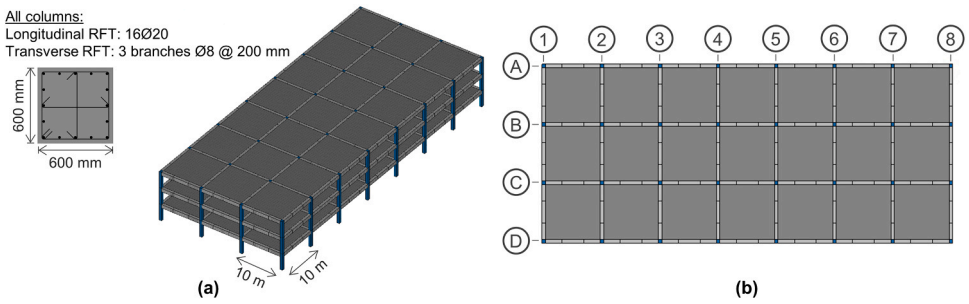

Fig. 7. (a) 3D model of prototype building and structural design of all columns; (b) Reference grid showing labels used to refer to column positions in this article.

Table 2
Summary of structural design of beams.

Location	Cross-section	Longitudinal reinforcement				Transverse reinforcement (Ø8)	
	Width × Depth [mm]	End zones		Middle zone (3.67 m)		End zones	Middle zones
		Top	Bottom	Top	Bottom		
All perimeter beams	600 × 800	10 Ø20	10 Ø20	10 Ø20	10 Ø20	4-legged @100 mm	4-legged @250 mm
Interior beams in outer bays (Floors 1 & 2)	600 × 800	8 Ø20	4 Ø20	2 Ø20	7 Ø20	3-legged @ 70 mm	3-legged @150 mm
Interior beams in inner bays (Floors 1 & 2)	600 × 800	9 Ø20	4 Ø20	2 Ø20	6 Ø20	3-legged @90 mm	3-legged @180 mm
Interior beams in outer bays (Floor 3)	600 × 800	6 Ø20	4 Ø20	4 Ø20	10 Ø20	3-legged @80 mm	3-legged @150 mm
Interior beams in inner bays (Floors 3)	600 × 800	9 Ø20	4 Ø20	4 Ø20	6 Ø20	3-legged @80 mm	3-legged @150 mm

class (DCL) was chosen for the design, which is suitable only for low seismicity cases. Concrete with a characteristic cylinder compressive strength of 30 MPa and B500S steel was specified. The resulting design of all columns is summarised in Fig. 7a, while the design of the beams is summarised in Table 2. The floors consist of a two-way slab with a thickness of 250 mm, a top reinforcing mesh with Ø12 mm bars at a spacing of 150 mm, and a bottom reinforcing mesh with Ø16 mm bars at a spacing of 100 mm. It is important to highlight that the cross-sectional area of continuity reinforcement only had to be changed significantly in the perimeter beams in order to comply with the requirements of the tying force method employed (see subsection 3.1). The reinforcement area in slabs of the first two floors based on the original design already complied with capacity requirements for internal ties.

3.1. Robustness design

As previously mentioned, the tying system in the prototype building was designed according to the rational horizontal tying force method [43] developed as a part of the CEN/TC 250 for the next generation of the Eurocodes. This proposed horizontal tying force method was developed based on a similar rationale for alternative load paths as that adopted in modern design codes such as the UFC 4–023-03 [7]. One of the main features considered in the method is that it explicitly accounts for the influence of the bridging system's ductility limit, which is expressed as a function of the rotation capacity. The method allows tying forces to be provided by the reinforcement in the beams, slabs, or a combination of both. This feature offers more freedom to practising engineers when compared to the current prescriptive method included in Eurocode 1 [9], theoretically allowing more optimised and cost-efficient robustness design. For the design of the prototype building, it was assumed that peripheral ties are fully provided by the reinforcement of the perimeter beams. In contrast, the internal ties are provided by the reinforcement in the two-way slab system.

The general formulation of the required tying forces is expressed below:

$$T \geq \mu\rho\left(\frac{i_f}{\overline{\alpha}}\right)P, \quad \overline{\alpha} = \frac{\alpha}{0.2} \quad (\alpha \text{ in rad}) \tag{1}$$

where $P = \sum P_j$ is the total equivalent load obtained as a superposition from all loads applied to the double-span beam/floor system, and $T = \sum T_k$ is the total equivalent tying force obtained as a superposition from all active tying forces within the beam/floor system. The other parameters are described in Table 3, along with the final values used for the design of the prototype building.

To determine an appropriate value of the rotation limit (α) and the dynamic amplification factor of the system, a nonlinear static (push-down) analysis was performed in SAP2000. This analysis adopted distributed fibre hinges for the beams and columns and nonlinear-layered shells for the floor slabs [46]. Specifically, static pushdown simulations of the two different column-removal scenarios shown in Fig. 8a were performed since they represent the least constrained (corner) and most constrained (internal) columns of the building. The predicted load-deflection responses from these simulations were extracted and converted into pseudo-static curves using the

Table 3
Summary of parameters employed in general formulation for tie force requirements.

Parameter	Description	Value used for internal ties	Value used for peripheral ties
i_f	Tying force intensity factor that depends on the system under consideration (determined based on the principle of virtual energy, equilibrating the internal force of the tying system with the external virtual work caused by the applied load.	3.125	2.5
α	Maximum rotation in radians (system ductility limit).	0.18	0.18
μ	Dynamic amplification factor allowing for the influence of the sudden column removal	1.25	1.25
ρ	Reduction factor that accounts for additional overstrength contributed by residual flexural resistance, strain-hardening of the rebar, and through-column reinforcement for a punching shear scenario.	1	1

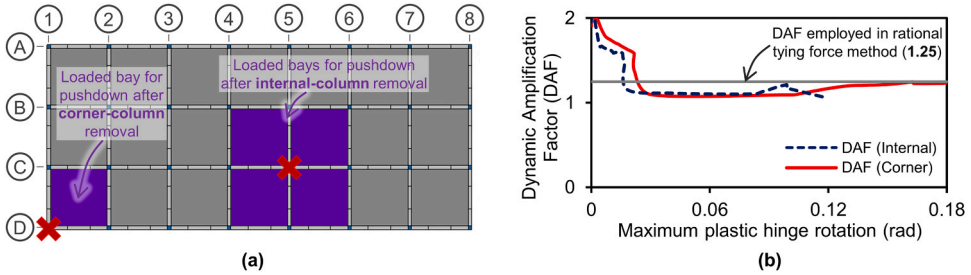

Fig. 8. (a) Column-removal locations and loaded bays used for nonlinear static pushdown and dynamic analyses used to compute dynamic amplification factor.

conservation of energy principle [47]. The dynamic amplification factors for different rotation levels estimated using this approach are plotted in Fig. 8b. As shown, the analysis indicates that 0.18 radians is a suitable value for the rotation limit of the system, with a dynamic amplification factor of 1.25 at that corresponding rotation. Although the nonlinear model used for the pushdown simulations can capture the beneficial effect of residual flexural resistance and membrane action of the slabs, these are not considered when computing the required reinforcement using a reduction factor (ρ) of 1 with the rational horizontal tying force method (subsections 3.1.1 and 3.1.2). Therefore, the continuity reinforcement requirements estimated using this method can be expected to be slightly conservative.

3.1.1. Tie force requirements for peripheral ties

According to the rational horizontal tying force method [43], the tying force intensity factor can be taken as 2.5 when tying forces can be achieved through double-span beams with a regular and symmetric span. Based on this assumption and the results of the pseudo-static analyses performed, the minimum required tying forces for the peripheral ties can be calculated as:

$$T_{per} = \mu\rho\left(\frac{i_{f,\,beam}}{\overline{\alpha}}\right)P_{per}$$

$$T_{per} = 1.25 \times 1\left(\frac{2.5}{\frac{0.18}{0.2}}\right)P_{per} = 3.47P_{per}$$

$$T_{per} = 3.47 \times 753\ kN \cong 2615\ kN$$

Assuming Ø20 bars made of B500S steel, the number of required continuity bars for the perimeter beam can be determined:

$$n_{per} = \frac{T_{per}}{A_s \times f_{yd}} = \frac{2615 \times 1000}{100\pi \times \frac{500}{1.15}} = 19.14 \cong 20\ bars$$

Thus, 10 Ø20 top bars and 10 Ø20 bottom bars were included in the design of the perimeter beams. This new configuration is higher than the number of bars required by the ULS combination (6 Ø20 top bars and 4 Ø20 bottom bars).

3.1.2. Tie force requirements for internal ties

For the two-way floor tying constituting the internal ties, the force intensity factor can be taken as 3.125 [43]. As a simplification, the same rotation limit and dynamic amplification factor used for calculating the peripheral ties was employed. This simplification is deemed reasonable as the building has a regular and simple layout, and the internal ties are implemented in the slab. Thus, the minimum required tying forces (calculated per m width of slab) for the internal ties can be determined as:

$$T_{\text{int}} = \mu\rho\left(\frac{i_{f,\,slab}}{\overline{\alpha}}\right)P_{\text{int}}$$

$$T_{\text{int}} = 1.25 \times 1\left(\frac{3.125}{\frac{0.18}{0.2}}\right)P_{\text{int}} = 4.34P_{\text{int}}$$

$$T_{\text{int}} = 4.34 \times 138\ kN/m \cong 599\ kN/m$$

Assuming Ø16 bars made of B500S steel, the spacing of the continuity bars to be distributed throughout the floor slab can be determined:

$$s_{\text{int}} = \frac{A_s \times f_{yd}}{T_{\text{int}}} = \frac{64\pi \times \left(\frac{500}{1.15}\right)}{599\ kN/m} = 146\ mm \cong 125\ mm$$

The original design of the slab already includes Ø16 with a spacing of 100 mm for the bottom bars, hence no modification is required. It is necessary to ensure that these bottom bars are installed continuously throughout the slab and anchored correctly in order to develop an effective tying mechanism.

4. Analysis of the role of continuity reinforcement in collapse propagation

In order to study how continuity reinforcement can contribute to pulling parts of a remaining structure during a collapse, a large initial failure scenario which results in collapse propagation was first identified (subsection 4.1). A very localised reduction in continuity was then introduced in the prototype design along carefully selected planes (subsection 4.2). The structural response of the original prototype design with full continuity was then compared to that of the modified design for the previously identified large initial failure scenario to assess the contribution of continuity reinforcement to collapse propagation (subsection 4.3). Finally, the performance of the modified design with reduced continuity after single-column failure was evaluated to verify if it significantly reduces the ability of the structural system to develop alternative load paths (subsection 4.4).

4.1. Collapse-propagation scenarios

First, it was verified that the prototype structure with full continuity would be able to survive the removal of single columns. This verification was performed using nonlinear dynamic simulations based on the AEM, the same strategy employed for all results presented in Section 4. Indeed, these simulations indicate that no collapse occurs after the removal of ground-floor columns at locations A1 (corner), A2 (penultimate-long edge), A4 (long edge), B1 (penultimate-short edge), B2 (interior-penultimate), and B4 (interior). The single-column removal scenario leading to the greatest vertical displacement at the removal location (95.20 mm) corresponds to the removal of column B1.

Several two-column failure scenarios were then investigated. For all the scenarios studied, partial collapse always occurred after the removal of two columns. However, the collapse was generally confined to the bays adjacent to the removed column. A similar phenomenon was observed after the removal of four columns as shown in Fig. 9.

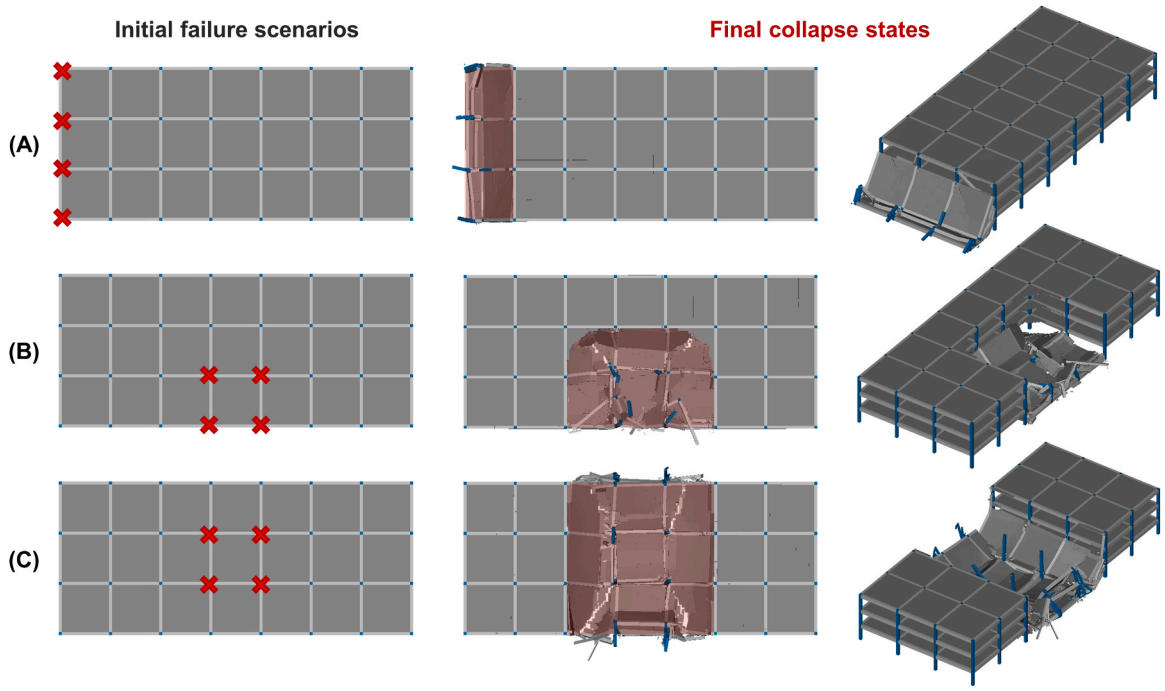

Fig. 9. Studied initial failure scenarios consisting of four-column removal.

A number of larger initial failures involving the loss of part of the building were also investigated by simulating the removal of 6 or 8 columns (see Fig. 10). The fact that initial failure scenario D led to a significantly greater extent of collapse compared to scenario E is unexpected, particularly considering that the columns removed in the former are a subset of those removed in the latter. It is likely that the asymmetric nature of the loads transferred by the collapsing parts in Scenario D contribute significantly to the greater extent of collapse observed in this case. This shows that the safety of remaining building segments after an initial failure depend on their boundary conditions and on the magnitude and symmetry of the loading imposed onto them by collapsing parts, underlining the case-specific nature of collapse propagation.

As can be observed in Fig. 10, the initial failure of the central part of the building (scenario F) leads to total collapse of the entire structure. As such, this scenario will be studied in further detail in subsection 4.3. Although very large (loss of 8 columns), it is worth mentioning that such an initial failure is not completely unconceivable, for example due to aircraft impact, sinkholes [48,49] or landslides [50,51]. It is also worth mentioning that the symmetric nature of scenario F makes it a good case to develop a more fundamental understanding of the role of continuity in collapse propagation.

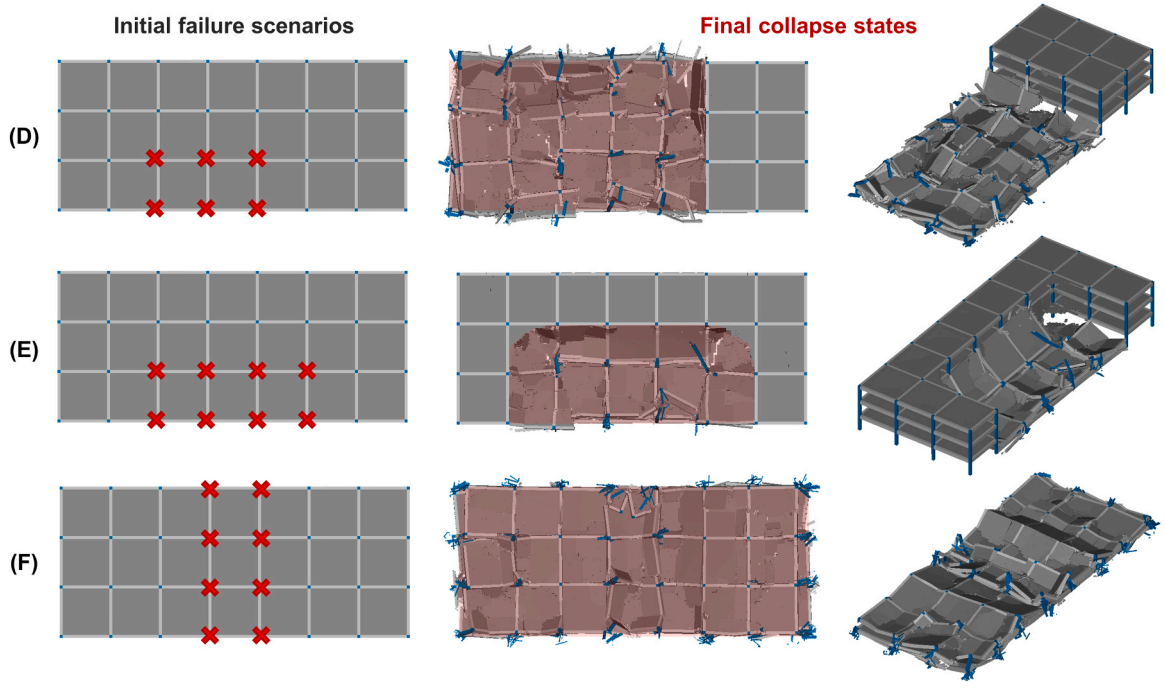

Fig. 10. Studied initial failure scenarios consisting of more than four columns.

4.2. Reduced continuity

As previously mentioned, a modified design involving localised reductions in continuity was defined in order to assess the influence of continuity on collapse behaviour. This was achieved by reducing the cross-sectional area of all the reinforcement over a length of 20 cm along the two planes shown in Fig. 11. These two planes were deemed suitable because they correspond approximately to the inflection point of the beams, which are not strained significantly by gravity loads under normal operational conditions. Only the minimum reinforcement as specified in ACI 318–19 [52] for beams and in slabs due to shrinkage and temperature effects was included at these locations. This corresponds to using only 6 Ø12 top bars and 5 Ø12 bottom bars in the beams. In the slabs, this was implemented by using Ø8 bars for both top and bottom reinforcement at the same spacing as in the original design. As a result, the reduced continuity building prototype still complied with requirements for ultimate limit state design. It should be noted that although the reduced continuity was implemented in the computational models using reduced bar diameters, a similar effect could be achieved in practice by cutting a selected number of bars per unit length along a specific plane.

4.3. Effect of reduced continuity on failure propagation

The predicted structural response of the two prototype building designs (full continuity and reduced continuity) after the removal of the 8 columns corresponding to initial failure scenario F are shown in Fig. 12.

For this initial failure scenario, it can be observed that full continuity leads to more unbalanced forces being transmitted to ground floor columns, which subsequently fail and lead to the total collapse of the structure. Closer examination of the collapse sequence reveals that the first column to fail after the initial removal of columns in the building with full continuity is column B7. This column fails approximately 0.50 s after the initial loss of columns (see Fig. 13), which triggers the subsequent failure of other columns as more unbalanced forces are redistributed to them.

To better understand the nature of the propagation mechanisms, the evolution of shear forces and bending moments in selected columns after the initial removal of columns (time= 0 s) were examined in greater detail in both prototype designs. Fig. 14 shows the time histories of bending moments and shear forces in an internal column one bay away from the removed column rows (C6), whereas Fig. 15 shows the same time histories for an internal column two bays away (C7). The estimated capacities without considering any strength reduction factors are also shown in these figures. In addition, the maximum values of shear forces and bending moments in these columns as well as in edge columns found in the same row of columns (D6 and D7) are summarised in Table 4 and Table 5. An estimate of the demand-to-capacity ratio (without any strength reduction factors) corresponding to the maximum values of these straining actions is also shown in the same tables. The capacity of the columns in shear was computed using the formulation proposed in ACI 318–19 [52] which also takes into account the current level of compressive stress in the column. The moment capacity was computed using an axial force-moment interaction diagram based on the strain distribution limits defined in Eurocode 2 [44].

It can be observed that the safety of columns in both the original design as well as that with reduced continuity is very similar up to the first triggering column failure, which occurs at approximately 0.5 s in the full continuity design. At that point in time, the most critical case is clearly that of internal columns two bays away from the rows of lost columns (see Fig. 15, Table 4, and Table 5), which are above capacity in terms of both shear and flexure in the full continuity design. This indicates that the coupled consideration of both these actions is important for estimating the first triggering failure, which is not significantly dominated only by shear or flexure individually.

The analysis suggests that the small reduction in continuity that was implemented reduced the forces being transmitted to the internal columns of row 7 just enough to avoid their failure. Nevertheless, it is worth saying that the peak values of shear and moment experienced by these columns are still very close to capacity. In fact, the maximum moment recorded in C7 for the reduced continuity design even exceeds capacity during the first surge of forces after column-removal (see Table 5). However, for combined axial and flexural failure modes, there is still significant residual capacity thanks to strain hardening of the rebars. In any case, the failure due to shear also appears to be very close to capacity, indicating that the safety of certain columns was still precarious in the reduced continuity design immediately after the loss of the columns.

Following the triggering failure of an internal column in row 7 that occurred in the full continuity design, there is a surge in the bending moments and shear in other columns which causes them to fail and the collapse to propagate. On the other hand, the shear forces and moments never rise again past the first significant peak in the reduced continuity design.

In general, for this building design, collapse propagation appears to be characterised more by failure due to combined axial and flexural actions rather than shear failure once the first triggering column failure occurs (after the initial loss of columns). It can be observed that the maximum bending moment in all columns occurs in the second surge after the triggering failure of column B7 (see time of occurrence in Table 5). In the case of shear, for the row of columns right next to the removed columns (row 6), the maximum shear occurs during the first peak, at the same time as the triggering column failure. On the other hand, for columns in row 7 behind row 6, the maximum shear always occurs during the second surge (see Table 4).

4.4. Performance of reduced continuity design after single-column failures

To evaluate the ability of the system with reduced continuity to accommodate alternative load paths (ALPs) and comply with robustness requirements in current standards, three single-column removal scenarios involving ground-floor columns closest to the reduced continuity location were investigated. The first scenario involved the removal of interior column C5, which is about ¾ of the span from the location of reduced reinforcement. The analysis indicated that the system prevented any local collapse, even with the weakening of the continuity.

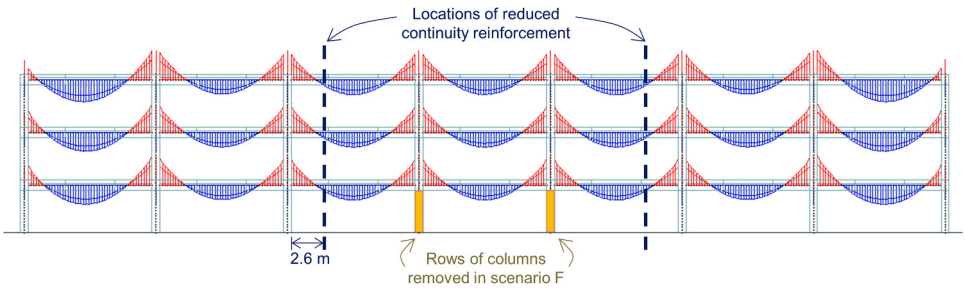

Fig. 11. Reduction in cross-sectional areas of reinforcement at inflection points of bending moments imposed by gravity loads.

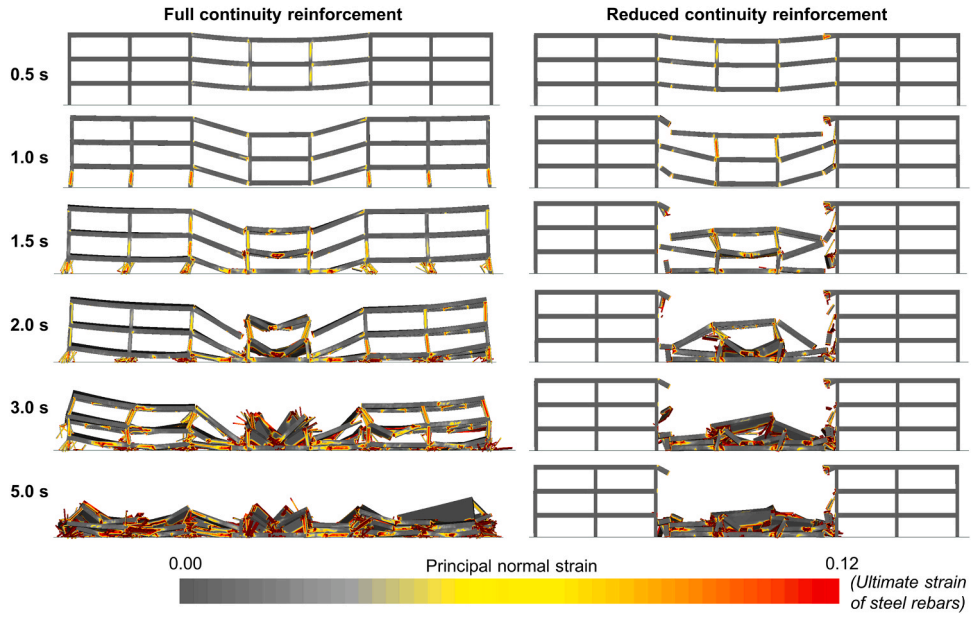

Fig. 12. Comparison of collapse progression between original design and design with reduced continuity reinforcement.

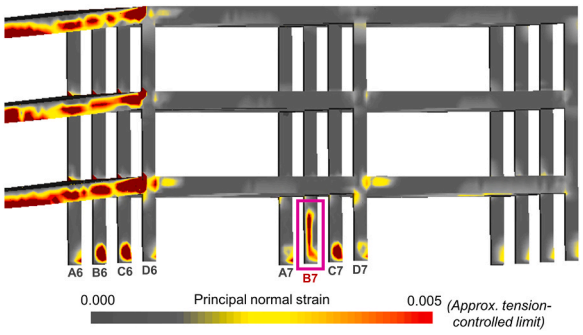

Fig. 13. Failure of column B7 0.52 s after the initial removal of columns (scenario F) in the building prototype with full continuity.

The bending moment distribution along the beams connected to the removed column and the variation of rebar stress at the location of the reduced continuity were extracted to investigate this phenomenon further.

The bending moment diagram shown in Fig. 16 indicates that the maximum demand (at the support location) is still lower than the beam's ultimate moment resistance, considering both flexural and arching action. The normalised compressive axial force ($P/A_g f_c^{'}$) extracted from the corresponding beams was computed to be between 0.1 and 0.2, indicating a significant contribution of arching action. This argument is also supported by the observation that the maximum vertical displacement of point C5 is 75 mm, corresponding to about 0.1 of the beam depth. This level of deflection is much lower than that necessary to activate catenary action (approximately equal to the beam depth). Thus, these two observations suggest that the system has not entered the catenary stage. The rebar stress at the location of the reduced continuity section is also shown in Fig. 16, which indicates that the bars are only experiencing small compressive stresses (about -40 MPa). This is expected as the reduced continuity location is still relatively close to the contraflexure point of the beam, even when column C5 is removed (see Fig. 16).

The second scenario investigates the removal of interior column C6, located about ¼ span away from the reduced continuity location. This particular scenario is considered as being more critical because it resulted in a significant increase in positive (sagging) bending moment at the location of reduced continuity. Fig. 17 shows the bending moment distribution in the third-floor beams surrounding the beam section with reduced continuity. The evolution of normal stresses in longitudinal rebars at the reduced continuity location is also shown.

In this case, the internal forces acting on the section with reduced reinforcement cause the maximum tensile stress of bottom bars to increase just enough for them to yield at this location. Nevertheless, the structural system with reduced continuity is still able to withstand the

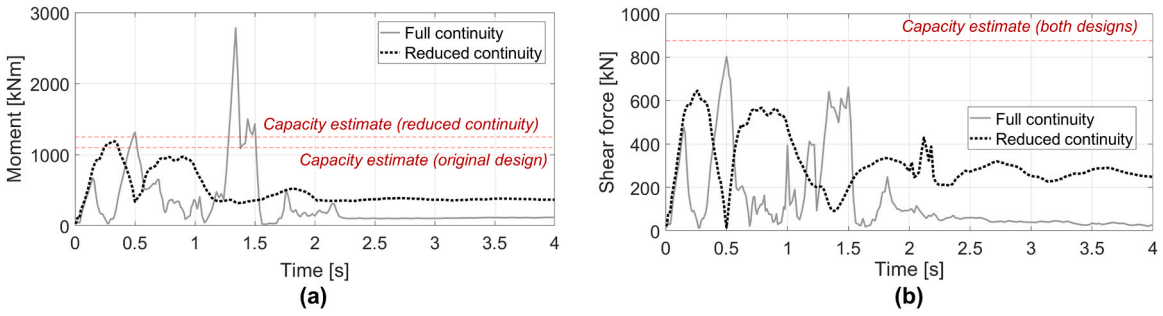

Fig. 14. Evolution of (a) maximum moment and (b) maximum shear in column C6. The shown capacity estimate for shear was computed according to the formulation proposed in ACI 318–19 with no strength reduction factor and considering the axial force at the time of the peak shear value. The capacity estimate for bending moment is based on the Eurocode 2 formulation with no strength reduction factors and considering the axial load at the time of the peak moment value.

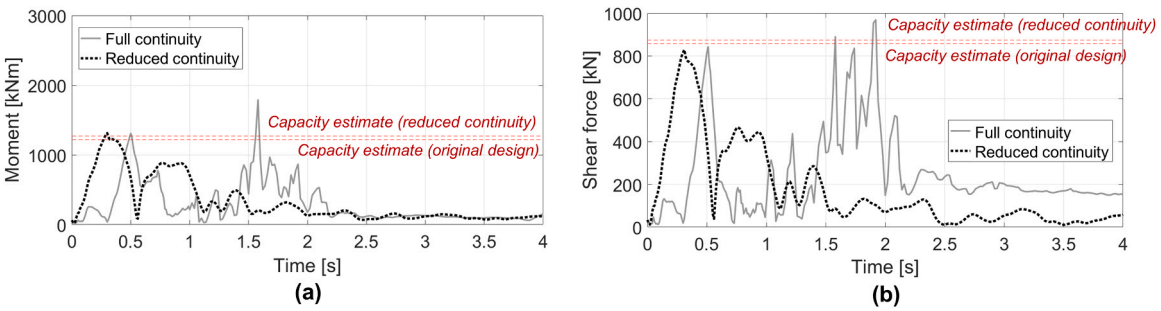

Fig. 15. Evolution of (a) maximum moment and (b) maximum shear in column C7. The shown capacity estimate for shear was computed according to the formulation proposed in ACI 318–19 with no strength reduction factor and considering the axial force at the time of the peak shear value. The capacity estimate for bending moment is based on the Eurocode 2 formulation with no strength reduction factors and considering the axial load at the time of the peak moment value.

Table 4
Summary of maximum shear force in key columns next to removed columns.

	Column C6		Column D6		Column C7		Column D7	
	Full continuity	Reduced continuity	Full continuity	Reduced continuity	Full continuity	Reduced continuity	Full continuity	Reduced continuity
Max. Shear force [kN]	803	645	691	643	969	829	1468	616
Time of occurrence [s]	0.50	0.26	0.54	0.29	1.92	0.31	2.02	0.34
Axial force at occurrence time [kN]	4795	4313	2546	2705	3368	5045	1203	2295
Demand-Capacity Ratio	0.92	0.74	0.94	0.85	1.13	0.95	2.75	0.88

Table 5
Summary of maximum bending moments in key columns next to removed columns.

	Column C6		Column D6		Column C7		Column D7	
	Full continuity	Reduced continuity	Full continuity	Reduced continuity	Full continuity	Reduced continuity	Full continuity	Reduced continuity
Max. Moment [kN]	2784	1189	1617	1046	1791	1314	1112	987
Time of occurrence [s]	1.34	0.33	1.50	0.27	1.58	0.30	2.00	0.34
Axial force at occurrence time [kN]	2784	4662	1822	2787	4183	5062	1129	2295
Demand-Capacity Ratio	2.53	0.95	1.65	0.95	1.47	1.04	2.12	0.95

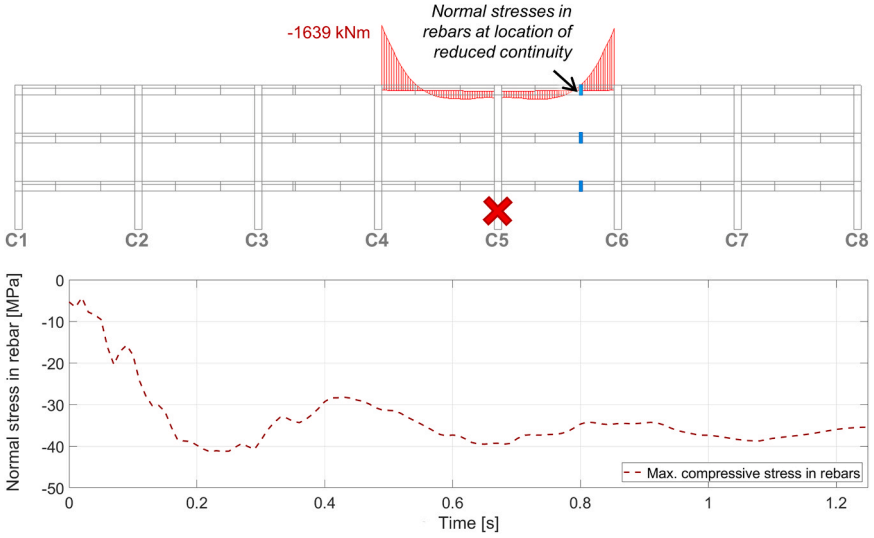

Fig. 16. Maximum normal stresses in rebars of third-floor beams at location of reduced continuity after removal of column C5. The bending moment diagram of the third-floor beams adjacent to the removed column is also shown.

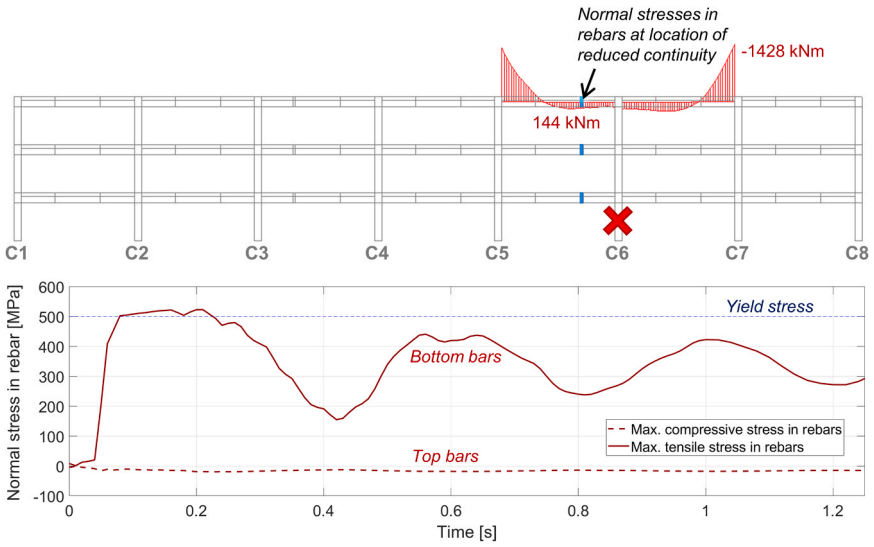

Fig. 17. Maximum normal stresses in rebars of third-floor beams at location of reduced continuity after removal of column C6. The bending moment diagram of the third-floor beams adjacent to the removed column is also shown.

removal of column C6 without any collapse.

The third scenario involved the removal of column D6, which represents edge columns closest to the location of reduced continuity (approximately ¼ span away). As shown in Fig. 18, the response of the structure following this column removal is similar to that following the removal of column C6. However, in this case, the bending moment at the reduced continuity location is smaller due to the smaller tributary area and load previously supported by the edge column. Despite this fact, the maximum tensile stress in bottom rebars at the reduced continuity location still peaks at a similar value as that observed following the removal of column C6. However, in this case, the residual effect of the straining actions acting at the reduced continuity location is less significant, as evidenced by the greater drop in positive tensile stresses following the initial peak. As such, for this particular structure and for the chosen segmentation configuration, the removal of edge column D6 can be considered as being less critical than the removal of interior column C6.

It should be noted that the removal of any other single column that is further away (e.g. corner columns) will be less critical for the reduced continuity location. This is because adjacent structural components to a removed column participate more in the development of alternative load paths. Therefore, less change from the straining actions in the undisturbed state will occur at the reduced continuity location compared to the changes in the column-removal scenarios shown in this Section.

Nevertheless, the magnitude of the increase in straining actions (and stress) at the reduced continuity location is case-dependent as it is affected by many factors, e.g., the magnitude of the gravity load, the building configuration and span length, and the stiffness ratio between the column and the beam-slab system. Therefore, although it was shown in this specific case study that the weakening of the section by assuming the minimum reinforcement ratio would still lead to compliance with the ALPM, the conclusions achieved here may not hold for other scenarios or building designs. Thus, performing an explicit check when determining the extent to which continuity can be reduced is important.

5. Conclusions

This article presents the results of an investigation into the possible

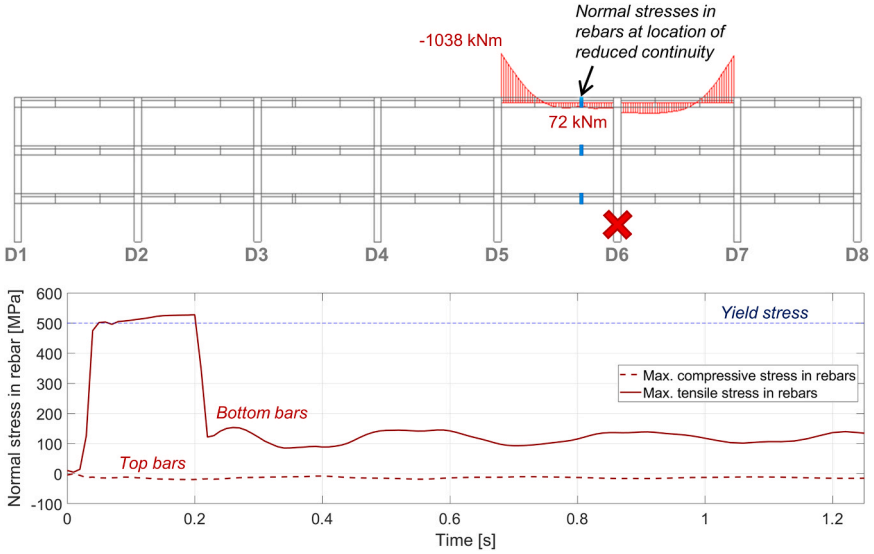

Fig. 18. Maximum normal stresses in rebars of third-floor beams at location of reduced continuity after removal of column D6. The bending moment diagram of the third-floor beams adjacent to the removed column is also shown.

contribution that continuity reinforcement can have on collapse progression. Several initial failure scenarios of a prototype building involving the loss of columns were investigated using a validated simulation strategy based on the Applied Element Method (AEM). The prototype building was found to be able to redistribute loads without collapse after the loss of single columns. On the other hand, one of two types of collapse occurred after larger initial failures: i) a partial collapse which only affected the bays directly adjacent to removed columns, or ii) a collapse which propagated to other parts of the structure, sometimes resulting in total collapse.

Further investigation revealed that for certain large initial failures, continuity reinforcement can contribute to the transmission of greater unbalanced forces to columns, causing them to fail and collapse to propagate.

It was demonstrated that reducing the amount of continuity reinforcement at certain locations can help arrest collapse propagation. In addition, it was also shown that this localised reduction of continuity reinforcement could still allow suitable alternative load paths (ALPs) to develop to avoid collapse after single-column failures, indicating that such modifications could still comply with robustness requirements in current standards. Nevertheless, the ability to develop these ALPs can be highly case-specific and will depend on both the positioning and amount of localised continuity reduction.

Results from this study suggest that there can be a certain optimal amount of continuity reinforcement, able to accommodate ALPs for single-column failure yet arrest the propagation of collapse when larger failures occur.

Declaration of Competing Interest

The authors declare that they have no known competing financial interests or personal relationships that could have appeared to influence the work reported in this paper.

Acknowledgements

This article is part of a project (Endure) that has received funding from the European Research Council (ERC) under the European Union's Horizon 2020 research and innovation programme (Grant agreement No. 101000396). Funding for open access charge: CRUE-Universitat Politècnica de València. The authors are also grateful to members of the ICITECH institute, and particularly Manuel Buitrago, for invaluable discussions on fuse-based segmentation.

References

[1] Russell JM, Sagaseta J, Cormie D, Jones AEK. Historical review of prescriptive design rules for robustness after the collapse of Ronan Point. Structures 2019;20:365–73. https://doi.org/10.1016/j.istruc.2019.04.011.
[2] The Institution of Structural Engineers (IStructE). Manual for the systematic risk assessment of high-risk structures against disproportionate collapse; 2013.
[3] The Institution of Structural Engineers (IStructE). Practical guide to structural robustness and disproportionate collapse in buildings; 2010.
[4] National Institute of Standards and Technology (NIST). NISTIR 7396: Best practices for reducing the potential for progressive collapse in buildings; 2007:216.
[5] FIB Commission 6. Guide to good practice: Design of precast concrete structures against accidental actions. Lausanne (Switzerland); 2012.
[6] Adam JM, Parisi F, Sagaseta J, Lu X. Research and practice on progressive collapse and robustness of building structures in the 21st century. Eng Struct 2018;173:122–49. https://doi.org/10.1016/j.engstruct.2018.06.082.
[7] Department of Defense (DoD). UFC 4-023-03. Design of buildings to resist progressive collapse. Des Build Resist Prog Collapse 2016:34–7.
[8] European Committee for Standardization (CEN). EN 1990:2002: Eurocode 0 - Basis of structural design; 2002.
[9] European Committee for Standardization (CEN). EN 1991-1-7:2006: Eurocode 1 - Actions on structures - Part 1–7: General actions - accidental actions; 2006.
[10] American Society of Civil Engineers (ASCE). Standard for mitigation of disproportionate collapse potential in buildings and other structures. Reston, VA: American Society of Civil Engineers; 2023. https://doi.org/10.1061/9780784415931.
[11] European Convention for Constructional Steelwork (ECCS). FAILNOMORE. D3–1: Design recommendations against progressive collapse in steel and steel-concrete buildings; 2021:244.
[12] Kiakojouri F, Zeinali E, Adam JM, De Biagi V. Experimental studies on the progressive collapse of building structures: a review and discussion on dynamic column removal techniques. Structures 2023;57:105059. https://doi.org/10.1016/j.istruc.2023.105059.
[13] Alshaikh IMH, Bakar BHA, Alwesabi EAH, Akil HM. Experimental investigation of the progressive collapse of reinforced concrete structures: An overview. Structures 2020;25:881–900. https://doi.org/10.1016/j.istruc.2020.03.018.
[14] Orton SL, Kirby JE. Dynamic response of a RC frame under column removal. J Perform Constr Facil 2014;28. https://doi.org/10.1061/(ASCE)CF.1943-5509.0000464.
[15] Kunnath SK, Bao Y, El-Tawil S. Advances in computational simulation of gravity-induced disproportionate collapse of rc frame buildings. J Struct Eng 2018;144:03117003. https://doi.org/10.1061/(ASCE)ST.1943-541X.0001938.
[16] Adam JM, Buitrago M, Bertolesi E, Sagaseta J, Moragues JJ. Dynamic performance of a real-scale reinforced concrete building test under a corner-column failure scenario. Eng Struct 2020;210:110414. https://doi.org/10.1016/j.engstruct.2020.110414.
[17] Buitrago M, Makoond N, Moragues JJ, Sagaseta J, Adam JM. Robustness of a full-scale precast building structure subjected to corner-column failure. Structures 2023;52:824–41. https://doi.org/10.1016/j.istruc.2023.03.146.
[18] Loizeaux M, Osborn AE. Progressive collapse—an implosion contractor's stock in trade. J Perform Constr Facil 2006;20:391–402. https://doi.org/10.1061/(ASCE)0887-3828(2006)20:4(391).
[19] Caredda G, Makoond N, Buitrago M, Sagaseta J, Chryssanthopoulos M, Adam JM. Learning from the progressive collapse of buildings. Dev Built Environ 2023;15:100194. https://doi.org/10.1016/j.dibe.2023.100194.
[20] Starossek U. Progressive collapse of structures. Second ed. ICE Publishing,; 2017. https://doi.org/10.1680/pcos.61682.
[21] Starossek U, Wolff M. Design of collapse-resistant structures. Watford: JCSS IABSE Work. Robustness Struct; 2005.
[22] Tanner P., Hingorani R. Robustness: A practitioner's perspective. IABSE Symp. Guimaraes 2019 Towar. a Resilient Built Environ. - Risk Asset Manag.; 2019, p. 1444–51. https://doi.org/10.2749/guimaraes.2019.1444.
[23] Makoond N, Buitrago M, Adam JM. Improving building robutness through fuse-segmentation. 6th Int Conf Prot Struct, Auburn 2023.
[24] Fallon CT, Quiel SE, Naito CJ. Uniform pushdown approach for quantifying building-frame robustness and the consequence of disproportionate collapse. J Perform Constr Facil 2016;30:4016060. https://doi.org/10.1061/(ASCE)CF.1943-5509.0000912.
[25] Scalvenzi M, Gargiulo S, Freddi F, Parisi F. Impact of seismic retrofitting on progressive collapse resistance of RC frame structures. Eng Fail Anal 2022;131:105840. https://doi.org/10.1016/j.engfailanal.2021.105840.
[26] Pantidis P, Cao L, Gerasimidis S. Partial Damage Distribution and Progressive Collapse of Buildings. Struct. Congr2020. Reston, VA: American Society of Civil Engineers; 2020. p. 52–62. https://doi.org/10.1061/9780784482896.006.
[27] Applied Science International. Extreme Loading for Structures - Theoretical Manual; 2021:108.
[28] Meguro K, Tagel-Din H. Applied element method for structural analysis: theory and application for linear materials. Doboku Gakkai Ronbunshu 2000;2000:31–45. https://doi.org/10.2208/jscej.2000.647_31.
[29] Tagel-Din H, Meguro K. Applied element method for dynamic large deformation analysis of structures. Doboku Gakkai Ronbunshu 2000;2000:1–10. https://doi.org/10.2208/jscej.2000.661_1.
[30] Tagel-Din H., Meguro K. Analysis of a small scale RC building subjected to shaking table tests using applied element method. Proc. Twelfth World Conf. Earthq. Eng., Auckland, New Zealand; 2000.
[31] Tagel-Din H, Meguro K. Applied element simulation for collapse analysis of structures. Bull Earthq Resist Struct 1999;32:113–23.
[32] Pham AT, Tan KH. Static and dynamic responses of reinforced concrete structures under sudden column removal scenario subjected to distributed loading. J Struct Eng 2019;145. https://doi.org/10.1061/(ASCE)ST.1943-541X.0002214.
[33] Grunwald C, Khalil AA, Schaufelberger B, Ricciardi EM, Pellecchia C, De Iuliis E, et al. Reliability of collapse simulation – comparing finite and applied element method at different levels. Eng Struct 2018;176:265–78. https://doi.org/10.1016/j.engstruct.2018.08.068.
[34] Xiao Y, Kunnath S, Li FW, Zhao YB, Lew HS, Bao Y. Collapse test of three-story half-scale reinforced concrete frame building. Acids Struct J 2015;112:429–38. https://doi.org/10.14359/51687746.
[35] American Society of Civil Engineers. ASCE 7-2002: minimum design loads for buildings and other structures. Reston, VA: Americans Society of Civil Engineers; 2002.
[36] Amercian Concrete Institute (ACI) Committee 318. Building Code Requirements for Structural Concrete (ACI 318–08) and commentary; 2007.
[37] Xiao Y, Zhao YB, Li FW, Kunnath S, Lew HS. Collapse test of a 3-story half-scale RC frame structure. Struct. Congr2013. Reston, VA: American Society of Civil Engineers; 2013. p. 11–9. https://doi.org/10.1061/9780784412848.002.
[38] Lertsrisakulrat T, Watanabe K, Matsuo M, Niwa J. Experimental study on parameters in localization of concrete subjected to compression. Doboku Gakkai Ronbunshu 2001;2001:309–21. https://doi.org/10.2208/jscej.2001.669_309.
[39] Nakamura H, Nanri T, Miura T, Roy S. Experimental investigation of compressive strength and compressive fracture energy of longitudinally cracked concrete. Cem Concr Compos 2018;93:1–18. https://doi.org/10.1016/j.cemconcomp.2018.06.015.

[40] Lee J, Lopez MM. An experimental study on fracture energy of plain concrete. Int J Concr Struct Mater 2014;8:129–39. https://doi.org/10.1007/s40069-014-0068-1.
[41] Makoond N., Buitrago M., Adam J. Progressive collapse assessment of precast reinforced concrete structures using the Applied Element Method (AEM). 6th Int. Conf. Mech. Model. Struct. Eng. (CMMoST 2021), Valladolid; 2021.
[42] Makoond N, Buitrago M, Adam JM. Tests on a Full-Scale Precast Building for Robustness Assessment. Struct. Congr2023. Reston, VA: American Society of Civil Engineers; 2023. p. 10–20. https://doi.org/10.1061/9780784484777.002.
[43] Izzuddin BA, Sio J. Rational horizontal tying force method for practical robustness design of building structures. Eng Struct 2022;252:113676. https://doi.org/10.1016/j.engstruct.2021.113676.
[44] European Committee for Standardization (CEN). EN 1992: Eurocode 2 - Design of concrete structures; 2004.
[45] EN 1991–1-1. Eurocode 1: Actions on structures. Part 1–1: Densities, self-weight, imposed loads for buildings; 2003.
[46] Computers & Structures Inc SAP 2000 - CSI Analysis Reference Manual v18; 2017.
[47] Izzuddin BA, Vlassis AG, Elghazouli AY, Nethercot DA. Progressive collapse of multi-storey buildings due to sudden column loss — Part I: simplified assessment framework. Eng Struct 2008;30:1308–18. https://doi.org/10.1016/j.engstruct.2007.07.011.
[48] Cennamo C, Angelillo M, Cusano C. Structural failures due to anthropogenic sinkholes in the urban area of Naples and the effect of a FRP retrofitting. Compos Part B Eng 2017;108:190–9. https://doi.org/10.1016/j.compositesb.2016.09.043.
[49] Gutiérrez F, Galve JP, Lucha P, Bonachea J, Jordá L, Jordá R. Investigation of a large collapse sinkhole affecting a multi-storey building by means of geophysics and the trenching technique (Zaragoza city, NE Spain). Environ Geol 2009;58:1107–22. https://doi.org/10.1007/s00254-008-1590-8.
[50] Luo HY, Zhang LL, Zhang LM. Progressive failure of buildings under landslide impact. Landslides 2019;16:1327–40. https://doi.org/10.1007/s10346-019-01164-0.
[51] Tiago P, Júlio E. Case study: damage of an RC building after a landslide—inspection, analysis and retrofitting. Eng Struct 2010;32:1814–20. https://doi.org/10.1016/j.engstruct.2010.02.018.
[52] American Concrete Institute. 318-19 building code requirements for structural concrete and commentary. American Concrete Institute; 2019. https://doi.org/10.14359/51716937.